

A unified framework for coarse grained molecular dynamics of proteins

Jinzheng Zhu¹ and Jianpeng Ma^{1,2,3, a)}

¹⁾Shanghai AI Laboratory, Shanghai, 200030, China

²⁾Multiscale Research Institute of Complex Systems, Fudan University, Shanghai, 200433, China

³⁾Zhangjiang Fudan International Innovation Center, Fudan University, Shanghai, 201210, China

(Dated: 27 March 2024)

Understanding protein dynamics is crucial for elucidating their biological functions. While all-atom molecular dynamics (MD) simulations provide detailed information, coarse-grained (CG) MD simulations capture the essential collective motions of proteins at significantly lower computational cost. In this article, we present a unified framework for coarse-grained molecular dynamics simulation of proteins. Our approach utilizes a tree-structured representation of collective variables, enabling reconstruction of protein Cartesian coordinates with high fidelity. The force field is constructed using a deep neural network trained on trajectories generated from conventional all-atom MD simulations. We demonstrate the framework's effectiveness using the 168-amino protein target T1027 from CASP14. Statistical distributions of the collective variables and time series of root mean square deviation (RMSD) obtained from our coarse-grained simulations closely resemble those from all-atom MD simulations. This method is not only useful for studying the movements of complex proteins, but also has the potential to be adapted for simulating other biomolecules like DNA, RNA, and even electrolytes in batteries.

I. INTRODUCTION

Molecular dynamics simulations are a vital tool for protein structure prediction and drug design¹. However, simulating the motions of large biological molecules with traditional MD methods is computationally expensive, requiring significant time and resources due to factors like system size and simulation timescale². Accelerating these computations is a key focus for computational chemists and biologists. Efforts are primarily directed towards two approaches: hardware and software improvements. In the hardware arena, traditional MD codes have been rewritten to leverage the parallel processing power of Graphics Processing Units (GPUs)³. Additionally, the development of supercomputers like Anton has significantly boosted computational speed⁴. On the software front, researchers employ enhanced sampling methods, such as replica exchange methods, to explore a wider range of configurations within the simulated system⁵. Additionally, coarse-grained MD simulations focus on capturing essential features of the system while averaging over less crucial details. This approach offers significant computational and conceptual advantages compared to more detailed all-atom models.

Coarse-grained methods face several challenges due to the inherent complexity of biological molecules like proteins. These challenges include capturing the intricate motions of protein backbones due to the presence of flexible side chains, loops, and disulfide bonds. Additionally, describing an implicit solvent environment that accurately reflects the crucial role of water molecules in stabilizing folded protein structures, particularly hydrophobic interactions, proves difficult with CG methods. To overcome these challenges, CG methods employ two main paradigms: "top-down" and "bottom-

up"⁶. The "top-down" CG method constructs collective variables (CVs) based on experimental observations, often leveraging thermodynamic data. In contrast, the bottom-up approach utilizes classical or empirical atomic models. It requires a deeper understanding of the underlying physics and chemistry. Here, researchers leverage knowledge of fundamental properties like bond lengths, bond angles, dihedral angles, and non-bonded interactions to derive a coarse-grained representation of the system.

Within the bottom-up paradigm of CG methods, researchers leverage the framework of statistical mechanics to define effective interactions, such as potential energies⁷. Over the past decades, several traditional coarse-grained methods have emerged, demonstrating significant improvements in capturing protein dynamics⁸⁻¹². The incorporation of machine learning (ML) techniques has further enhanced the performance of CG simulations^{10,13,14}. For instance, Zhang et al. employed deep neural networks (DNNs) to approximate potential energy surfaces from coarse-grained coordinates, achieving consistent distributions of collective variables compared to those obtained from original MD simulations¹⁵. This framework further enabled enhanced sampling of large proteins¹⁶.

The three-dimensional structure of a protein, crucial for its function, is determined by an interplay between fixed covalent bonds and flexible internal angles. Among these internal angles, torsion angles (also known as dihedral angles) exhibit a more significant influence on protein conformation compared to the relatively static bond angles. Torsion angles display substantial fluctuations during MD simulations, significantly impacting how a protein folds. Consequently, these torsion angles are frequently incorporated into CG representations. Electron orbital hybridization dictates the preferred geometries of bond angles (e.g., sp^3 or sp^2). However, experimental observations and MD simulations reveal slight deviations from these ideal values. These deviations can be particularly significant when attempting to reconstruct

^{a)}Corresponding author email: jpm@fudan.edu.cn

a protein structure solely based on torsion angles. The error accumulates with each amino acid residue, as the position of an amino acid is dictated by the conformation of the preceding residues in the polypeptide chain. Therefore, CG representations that solely employ torsion angles are useful for obtaining a general understanding of a protein's backbone conformation or predicting side-chain structures (as demonstrated in references^{15,17,18}). However, they are inadequate for high-precision tasks such as complete protein structure prediction. For instance, the AlphaFold 2 (AF2) framework utilizes torsion angles for side-chain prediction but employs Cartesian coordinates for backbone prediction¹⁹. Recent work by Kohler et al. highlights the potential benefits of incorporating bond angles. Their CG model utilizes both torsion and bond angles for the central carbon (CA) atoms, successfully capturing protein folding/unfolding transitions in small systems²⁰. However, this approach does not capture the detailed dynamics of all the atoms and side chains within a protein.

In this research, we present a unified and recursive framework for constructing a bidirectional map between protein Cartesian coordinates and a minimal set of interpretable coarse-grained collective variables. This framework incorporates all heavy atoms in the backbone and side chains, enabling a comprehensive representation of the protein structure. Notably, our approach allows MD simulations to be performed solely using the collective variables, eliminating the need for explicit Cartesian coordinates. This significantly accelerates simulations while maintaining consistent performance with all-atom MD simulations, as measured by collective variable distributions and RMSDs at most time steps. Compared to existing methods that achieve only overall statistical consistency on collective variables¹⁵, our framework offers the advantage extra high accuracy in time series of RMSDs.

II. METHODS

A. Collective variables

1. coordinate transformation matrix

Our protein representation begins with a general description of atomic coordinate hierarchy in chemical compounds. For clarity, this work adopts a non-standard notation. The symbol ψ will represent any dihedral angle and φ will represent any bond angles. According to references²¹, the operating matrix $\hat{R}(\hat{u}, \theta)$ for rotating θ along a normalized rotation vector $\vec{u} = [\vec{u}_x, \vec{u}_y, \vec{u}_z]^T$ is

$$\begin{bmatrix} \vec{u}_x^2(1 - \text{cn}) + \text{cn} & \vec{u}_x\vec{u}_y(1 - \text{cn}) - \vec{u}_z\text{sn} & \vec{u}_x\vec{u}_z(1 - \text{cn}) + \vec{u}_y\text{sn} \\ \vec{u}_x\vec{u}_y(1 - \text{cn}) + \vec{u}_z\text{sn} & \vec{u}_y^2(1 - \text{cn}) + \text{cn} & \vec{u}_y\vec{u}_z(1 - \text{cn}) - \vec{u}_x\text{sn} \\ \vec{u}_x\vec{u}_z(1 - \text{cn}) - \vec{u}_y\text{sn} & \vec{u}_y\vec{u}_z(1 - \text{cn}) + \vec{u}_x\text{sn} & \vec{u}_z^2(1 - \text{cn}) + \text{cn} \end{bmatrix} \quad (1)$$

where \hat{I} is the identity matrix, $\text{sn} = \sin \theta$ and $\text{cn} = \cos \theta$. Considering the transformation, the general formula of coordinate transformation goes as a 4×4 matrix, where $\vec{0}$ is a 3×1 vec-

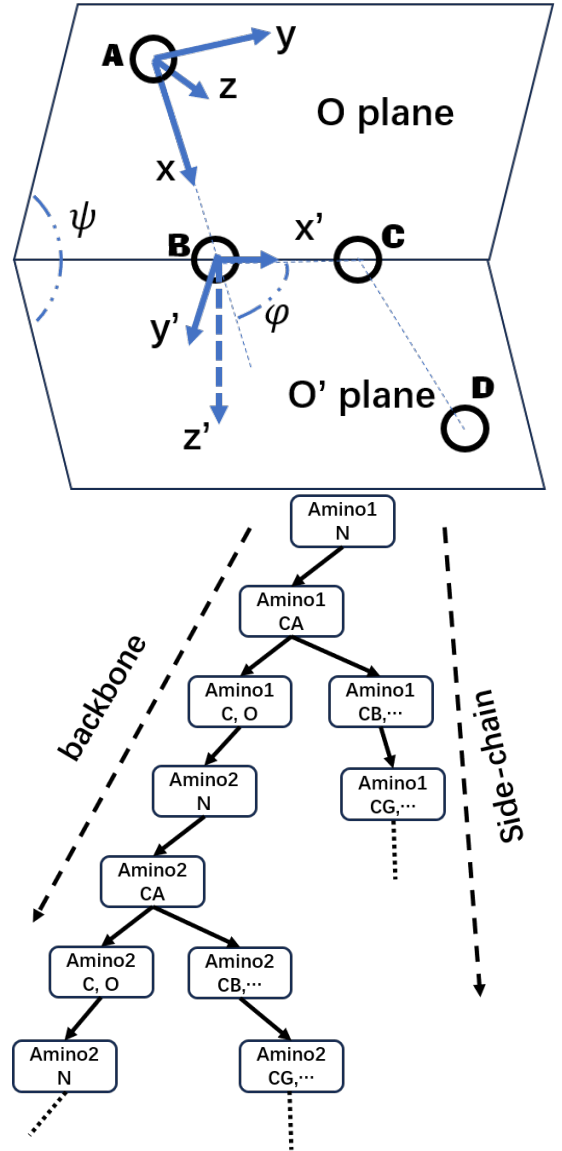


FIG. 1: This illustration depicts coordinate transform (upper) and tree structure of collective variables of atoms in proteins (lower) illustration.

tor filled with zeros and \vec{T} is a 3×1 matrix representing the translation.

$$\hat{M}(\vec{u}, \theta, \vec{T}) = \begin{bmatrix} \hat{R}(\hat{u}, \theta) & \vec{T} \\ \vec{0}^T & 1 \end{bmatrix} \quad (2)$$

Converting the coordinates in local axis frame ($x'y'z'$) to parent axis (xyz) can be understood as transforming the parent axis data (axis vector and the origin) to the local axis data in the parent axis frame, as illustrated in Fig. 1. This process includes three steps with operator written as

$$\hat{O} = \hat{M}_3 \hat{M}_2 \hat{M}_1 \quad (3)$$

, where first, \hat{M}_1 translates the frame along x axis by bond length l_b where $\hat{R}(\hat{u}, \theta) = \hat{I}$ and $\vec{T} = [0, 0, l_b]^T$; second, \hat{M}_2

rotates the frame along the new z axis by bond angle with $\theta = \varphi$, $\vec{T} = \vec{O}$ and $\vec{u} = [0, 0, 1]^T$; third, \hat{M}_3 rotates the frame along the new x axis by dihedral angle with $\theta = \psi$, $\vec{T} = \vec{O}$ and $\vec{u} = [1, 0, 0]^T$.

For complex molecules like proteins, multiple coordinate frames are used. One frame serves as the "global" reference, and data from other frames are transformed to this reference frame. The operator for obtaining the coordinates in current local frame to the given frame is denoted as

$$\hat{P}_{I,J} = \prod_{i=I+1}^J \hat{O}_i, 1 \leq I < J \quad (4)$$

with index showing the coordinate frames before current frame, and I and J being the target and current frame index. We denote the global operator for converting current coordinates to the "global" reference as

$$\hat{P}_I = \hat{P}_{I,1} = \hat{P}_{I-1} \hat{O}_I. \quad (5)$$

This approach leverages a recursive formula to efficiently compute the global transformation matrix for each reference frame. This eliminates the need for repeated calculations on individual sub-coordinates, simplifying the computational process. Consequently, equation

$$\vec{X} = \hat{P}_I \vec{x}^0, \vec{X} = [\vec{x}^T, 1]^T, \vec{x}^0 = [x^0{}^T, 1]^T \quad (6)$$

can be readily applied to determine any protein atom's Cartesian coordinates within the global reference frame, where vector \vec{x} and \vec{X} are original Cartesian coordinates (3×1) and extended coordinates (4×1). For convenience, subscript I indicates the number and index of coordinate transformation from the "global" coordinate. A superscript of "0" denotes a "local" coordinate within its frame, otherwise it's a "global" coordinate. As \vec{x}^0 are only determined by the amino type, the Cartesian coordinates \vec{x} are only dependent on \hat{P}_N . The bond lengths, l_b , used in the calculations can also be retrieved from a the standard amino acid structures. It is noteworthy that the connections between amino acids in a protein's backbone, specifically between the nitrogen and carbon atoms, have a fixed length of about 1.32 angstroms.

The conversion between a protein's 3D structure (Cartesian coordinates) and its internal torsion and bond angles is straightforward and is neglected here. This establishes a bidirectional mapping, facilitating analysis from both perspectives. To optimize computational efficiency, calculations consider only the essential heavy atoms. Additionally, rigid moieties like benzene rings require only two angles for complete description. This significantly reduces the number of variables needed, streamlining computational demands. While introducing some additional parameters compared to traditional methods, our approach offers substantial advantages. It allows reconstruction of the complete 3D structure, including side chains, leading to more accurate force field predictions – crucial for molecular simulations.

2. Tree data structure

Recursive data structures naturally lend themselves to representation using tree structures. This approach has been

successfully implemented in J. Zhu's prior work on quantum physics²²⁻²⁴. Similarly, the coordinates of each reference frame within a protein can be effectively represented as a tree structure, as demonstrated in Fig. 1. In this tree, each data node inherits its information from its parent node. This tree-based representation not only captures the hierarchical relationships between protein components but also partially incorporates the protein's geometric information. For a more detailed breakdown of the hierarchy within each amino acid, please refer to Table I in the appendix.

While the recursive multiplications of matrices can be computationally expensive, the reconstruction of protein 3D structures is only required during trajectory analysis. This means these computationally intensive operations are not necessary for real-time molecular dynamics simulations, thereby minimizing their impact on overall performance. Furthermore, the reconstruction of collective variable trajectories can be efficiently parallelized across CPUs and GPUs. This distributed processing approach effectively mitigates the performance drawbacks associated with recursive computation time.

B. Force field and molecular dynamics

Simulating large biomolecular systems necessitates capturing their statistical behavior. There exist two main approaches exist: stochastic methods and equilibrium sampling. Stochastic methods introduce random noise at each simulation step to mimic statistical fluctuations, starting from a defined initial state. Examples include Monte Carlo, random walk, and diffusion methods. Equilibrium sampling uses an initial state that already reflects the desired statistical properties, followed by noise-free simulations. This approach is employed in traditional MD simulations. Our work aligns with the second strategy (equilibrium sampling) by utilizing a machine learning force field trained on MD outputs. In contrast to methods that learn the energy landscape from existing trajectories, our approach directly predicts the next MD coordinate. This is possible because the statistical uncertainty is already embedded within the initial velocity distribution used during training. Subsequent steps involve solving Newton's equations of motion, efficiently leveraging the learned velocity information. The network's ability to predict the next coordinate while capturing statistical behavior becomes evident in the loss function design (Eq. 13, $n \geq 2$). This design trains the network on a sequence of consecutive frames, effectively capturing velocity and force field information from training data. Consequently, the task becomes one of predicting the next CVs based on the previous step, as the network has already learned the underlying statistical dynamics.

For all Cartesian coordinates transformation, Eq. 6 can be written as

$$\mathfrak{R} = \mathbb{P}(\vec{\theta}, \mathfrak{R}^0) \quad (7)$$

for N Cartesian coordinates $\mathfrak{R} = [\vec{x}_1, \vec{x}_2, \dots, \vec{x}_N]^T$ with their corresponding constant local coordinates $\mathfrak{R}^0 = [x^0_1, x^0_2, \dots, x^0_N]^T$, M pairs of collective variables

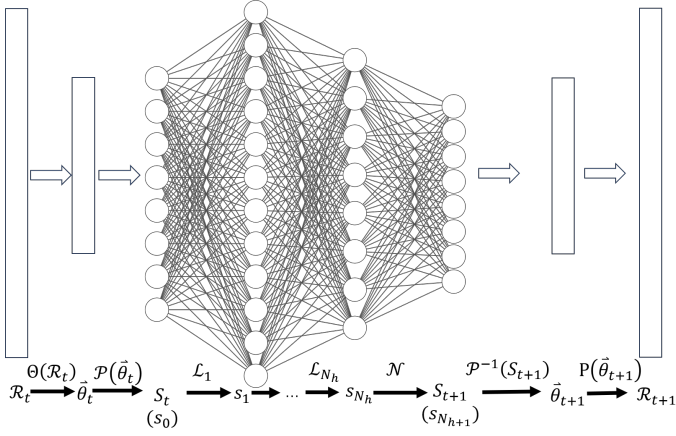


FIG. 2: Deep neural network architecture for predicting next protein coordinate.

$\vec{\theta} = [\psi_1, \psi_2, \dots, \psi_M, \varphi_1, \varphi_2, \dots, \varphi_M]^T$, and the overall operator \mathbb{P} being a combination of all the global operators \hat{P}_i . The inverse transformation for obtaining all the angles is written as

$$\vec{\theta} = \hat{\Theta}(\mathfrak{R}). \quad (8)$$

To overcome the periodicity of angles, in the network we project angles to sine-cosine values as

$$\mathbf{S} = \mathcal{P}(\vec{\theta}) = [\cos \psi_1, \dots, \cos \psi_M, \sin \varphi_1, \dots, \sin \varphi_M]^T. \quad (9)$$

The network's task is now to predict the subsequent collective variables based on the current ones. These predicted variables are also projected to sine-cosine values, formulated as

$$\mathbf{S}_{t+1} = \mathcal{F}(\mathbf{S}_t) = \mathcal{N} \circ \mathcal{L}^{N_h} \circ \dots \circ \mathcal{L}^1(\mathbf{S}_t) \quad (10)$$

, where N_h denotes the number of hidden layers in the network, t and $t+1$ represent the time indices (timestamps) of the trajectory data. The formula of function \mathcal{L}_d in each layer is written as

$$\mathbf{s}_d = \mathcal{L}_d(\mathbf{s}_{d-1}) = \mathcal{A}(\mathbf{W}_d \mathbf{s}_{d-1} + \mathbf{b}_{d-1}) \quad (11)$$

, where $\mathbf{W}_d \in \mathbb{R}^{M_d \times M_{d-1}}$ and $\mathbf{b} \in \mathbb{R}^{M_d}$ are weights to be learnt, and \mathcal{A} are activation functions. Our network distinguishes itself from Zhang et.al's¹⁵ work by introducing a normalization constraint, denoted by \mathcal{N} , for the sine-cosine operation within the network. This normalization step helps mitigate potential artifacts arising from the projection of angular data into sine and cosine components. While these constraints could also be incorporated into the loss function, we found that applying them directly through \mathcal{N} significantly accelerates the convergence of the network during training.

The task is to obtain the weights $\{\mathbf{W}_d, \mathbf{b}\}$ that minimize the loss that can be described as $\min_{\{\mathbf{W}, \mathbf{b}\}} L_T$. We use mean square error as the loss function which goes as

$$L_T = \frac{\sum_{t=1}^{T-1} |\mathbf{S}_{t+1} - \mathcal{F}(\mathbf{S}_t)|^2}{T-1} \quad (12)$$

, where we use error between variables at $t+1$ and those obtained from t . This loss can also be extended to a more general form as

$$L_{T_n} = \frac{1}{n} \sum_{i=1}^n \frac{1}{T-i} \sum_{t=1}^{T-i} \left| \mathbf{S}_{t+i} - \overbrace{\mathcal{F} \circ \dots \circ \mathcal{F}}^i(\mathbf{S}_t) \right|^2, 1 \leq n \leq T-1 \quad (13)$$

, where the error computed from subsequent coordinates after $t+1$ are also used. It is easy to see Eq. 13 collapses to Eq. 12 with $n=1$. Interestingly, when $n \geq 2$ in Eq. 13, the network effectively learns the underlying physical form of the force field. The velocity-verlet algorithm, a popular method in molecular simulations, allows for efficient calculation of forces acting on particles. This method uses the particles' positions at three time steps ($t-1$, t , and $t+1$) as detailed in

$$\begin{aligned} \mathbf{F}(\mathbf{S}_t) &= \mathbf{M}_S \times \mathbf{a} \approx \mathbf{M}_S \times \frac{\mathbf{S}_{t+1} + \mathbf{S}_{t-1} - 2\mathbf{S}_t}{\Delta t^2} \\ &= \mathbf{M}_S \times \frac{\mathcal{F} \circ \mathcal{F}(\mathbf{S}_{t-1}) + \mathbf{S}_{t-1} - 2\mathcal{F}(\mathbf{S}_{t-1})}{\Delta t^2}. \end{aligned} \quad (14)$$

The calculation works regardless of the particles' initial velocities. In Eq. 14, \times is the piece-wise multiplication operator, \mathbf{M}_S represents a constant mass assigned to each simplified unit (coarse-grained coordinate), Δt is the predefined time step, and the acceleration vector \mathbf{a} is the only unknown variable to be solved for. Thus including data from at least three successive trajectories enables the network to learn the force field information.

We employed two key strategies to assess the quality of the generated MD trajectories. First, we analyzed the statistical performance of all the CVs, similar to many other studies. This involved plotting the error bars associated with these CVs. Second, we quantified the overall structural similarity between the generated and reference trajectories by calculating the RMSD difference ($\Delta \text{RMSD}(t)$) between the predicted and reference RMSD values at each time step (t)

$$\Delta \text{RMSD}(t) = |\text{RMSD}(t) - \text{RMSD}_{Ref}(t)|. \quad (15)$$

The reference RMSD (RMSD_{Ref}) was obtained from the Cartesian coordinates.

III. APPLICATION

A. Protein Structure reconstruction

To evaluate the effectiveness of our coarse-grained methods, we selected a challenging protein target: the 168-amino acid protein T1027 (sequence: KPTENNEDFNIVAVASNFATDLDADRGLPGKKLPL-EVLKEMEANARKAGCTRGCLICLSHIKCTPKMKKFIP-GRCHTYEGDKESAQGGIGEAIVDIPAIPRFKDLPEMQFIAQVDLCVDCTTGCLKGLANVQCSDLLKKWLPQR-CATFASKIQGVQDKIKGAGGD) from the CASP14 prediction sets^{25,26}. This protein presents a computational challenge for traditional MD simulations due to its relatively

long sequence and the presence of free loops. Successfully predicting the motion of this protein using our coarse-grained approach would provide a robust validation of our methods' ability to handle complex protein dynamics.

Our coarse-grained representation utilizes 1624 parameters (described in Section II). This includes 812 bond angles and 812 dihedral angles, both on the backbone and side-chains. Compared to the 7665 parameters needed for a single protein's Cartesian coordinates and the significantly larger number required for full MD simulations (presented in Section III B), our approach offers a substantial reduction in dimensionality. The total number of CVs is larger than the representation using all dihedral angles for backbones that requires 504 parameters (3 angles/residue * 168 residues). This is because we include the corresponding bond angles and related side chain information. This additional complexity allows for a more precise and bidirectional representation of the protein structure.

Fig. 3 depicts the reconstructed initial structure of protein T1027. The reconstructed tertiary structure (cyan) exhibits a near-native match with the original data (gray), highlighting the accuracy of our approach. For comparison, the blue structure was built using all angles except for the sp^3 bond angles, which were fixed at their theoretical value ($109^\circ 28'$). This comparison reveals a significant mismatch, including the absence of part of the alpha helix. This demonstrates the substantial impact of even small variations in bond angles on protein structure, emphasizing the importance of including them in our representation. The secondary structure representation also shows good agreement between the reconstructed structure and the original data, with only minor deviations observed at the ends of a few amino acid side chains. Specifically, analysis of CA atom distances reveals a maximum deviation of 0.26 angstrom, with an average value of 0.04 angstrom. The maximum difference for side-chain atoms is 0.6 angstrom, with a mean of 0.26 angstrom. It is noteworthy that we utilize local coordinates (denoted as x^0 - see Section II A) for each amino acid, retrieved from a separate database independent of the T1027 structure. This approach can introduce slight error accumulation along the protein chain backbone, which can then propagate to the side chains (whose positions are highly dependent on the backbone). However, as will be shown in subsequent sections, the errors introduced by our coarse-grained representation remain consistently below 0.2 angstrom in practical applications, making them effectively negligible.

B. MD trajectories prediction

We employed the GROMACS²⁷⁻²⁹ software (version 2022.2) for the MD simulations, utilizing a timestep of 1 femtosecond (fs) and saving trajectories every 0.05 nanoseconds (ns). To enhance the efficiency of the simulations, we implemented an in-house developed enhanced sampling method, parallel continuous simulated tempering and a structure based model (PCST+SBM), within GROMACS. For a detailed description of PCST+SBM, please refer to refer-

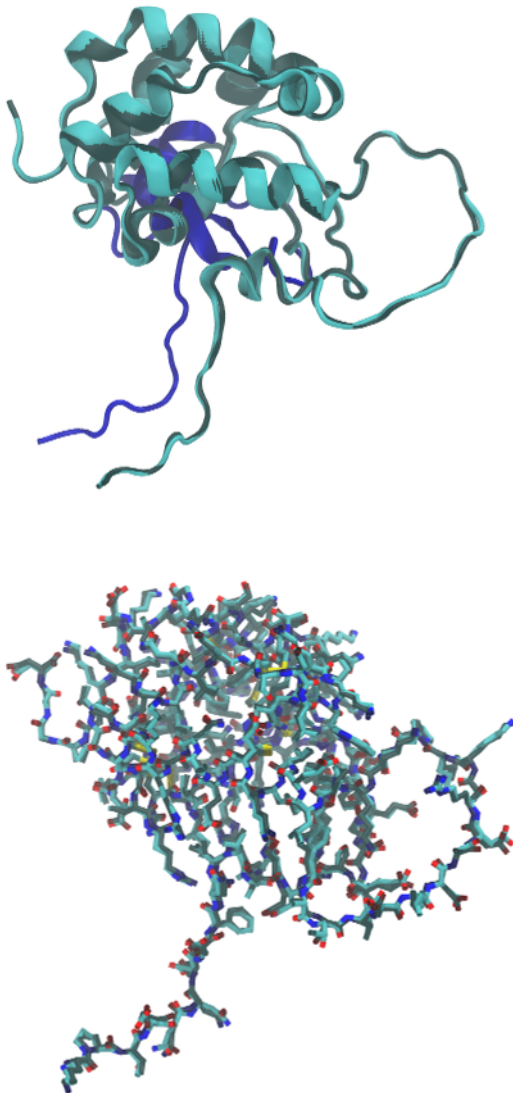


FIG. 3: Cartesian coordinates reconstruction using dihedral and bond angles. The upper figure compares the tertiary structures and the lower one compares the secondary structures that show side-chains consistency. The original 3D structure is colored gray and the green structure is constructed by all real dihedral and bond angles. The blue tertiary structure on the upper figure is constructed by all the real angle data except sp^3 bond angles are fixed to 1.29 rad($109^\circ 28'$).

ences³⁰⁻³³. We start the MD simulations from the refinement target in CASP14. Two copies are simulated in PCST, whose temperature distribution is defined by $\beta_0 = 0.38$, $\sigma_0 = 0.05$ and $\beta_1 = 0.27$, $\sigma_1 = 0.13$, respectively. In configuring the SBM method, we selected the starting target structure as the reference to promote initial-state fidelity during the MD simulations. This ensures the dynamics primarily focus on explor-

ing configurations near the initial structure. Compared to the original SBM implementation, we introduce a targeted constraint strategy. We constrain only the "slow" residues, which are crucial for calculating the RMSDs. Residues within loops are left unconstrained to facilitate efficient exploration of the conformational space.

For dataset preparation, we carefully select data points from the saved trajectories. Since the prediction of coordinates is inherently time-dependent, the data are sorted chronologically. Additionally, we address the artificial discontinuity introduced by replica exchange steps within the PCST method³². These exchanges, motivated by temperature differences, are not representative of the actual physical system governed by the force field. Therefore, we re-arrange the trajectories to create a continuous data stream for training. This ensures the DNN learns the underlying dynamics without being confounded by non-physical artifacts.

For training the deep neural network, we employ a common data split strategy: 70% of the processed trajectories are used for training, 20% for validation, and the remaining 10% for testing. We configure the network architecture with three hidden layers ($N_h = 3$) and utilize two weight matrices (M_d) of size 3248×3807 and 3807×3248 (details on weight matrix dimensions might be specific to your field). Our DNN network exhibits remarkable efficiency. It can generate a 25ns trajectory using only the initial structure as input and applying the network recursively to predict subsequent coordinates. This process takes merely 0.59 seconds on a standard NVIDIA GeForce GTX 1660 Ti (6G) GPU. In stark contrast, traditional MD simulations on a 256-CPU supercomputer require roughly 20 hours to generate a comparable trajectory. This translates to an impressive speedup of approximately 10,000 times achieved by the DNN network. Even when considering the training time (around 2 hours), the coarse-grained DNN network offers a significant speedup factor of 10 for the entire process. It's important to note that training can be further optimized by leveraging parallelization techniques and better GPUs.

Fig. 4 depicts the predicted performance of the MD simulation. The upper panel shows the angles (torsion angles ψ and bond angles $\pi - \varphi$). As expected, the ψ angles (represented in the first half) exhibit a wider distribution range due to their inherent flexibility in the protein backbone. In contrast, the φ angles ($\pi - \varphi$, shown in the second half) primarily cluster around 1.23 radians ($109^\circ 28'$) with a smaller variance (0.4 radians) during the simulation. This finding reinforces the earlier observation of bond angle fluctuations within MD simulations. Notably, a small population of φ angles around $\frac{2\pi}{3}$ radians likely originates from the carbonyl oxygen atoms in the backbone. The comparison of the orange (black) and red (predicted) curves reveals a high degree of consistency between the predicted statistical behavior of the angles and the original values. Similar observations can be made when analyzing the sine and cosine components of these angles, as presented in Fig. 5 in the appendix.

The RMSD values calculated from the predicted CVs closely match those obtained from the original Cartesian coordinates (Fig. 4, black vs. red lines). Our observations align

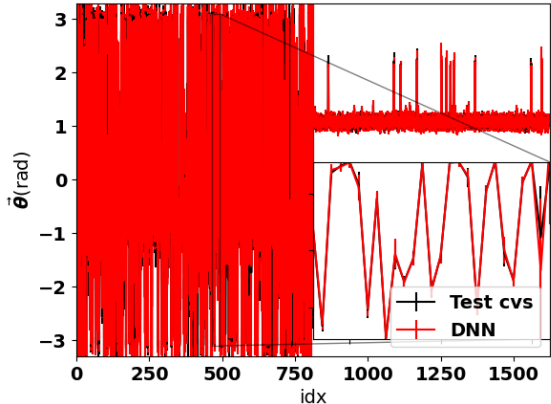
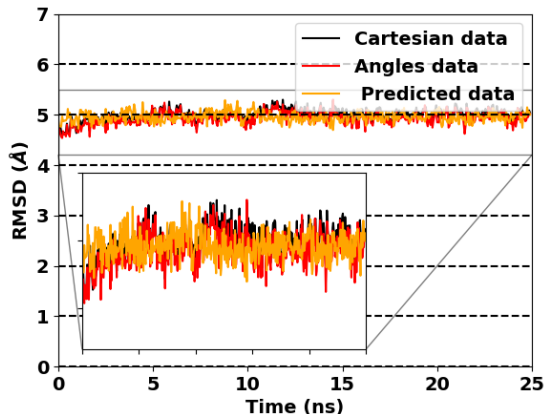
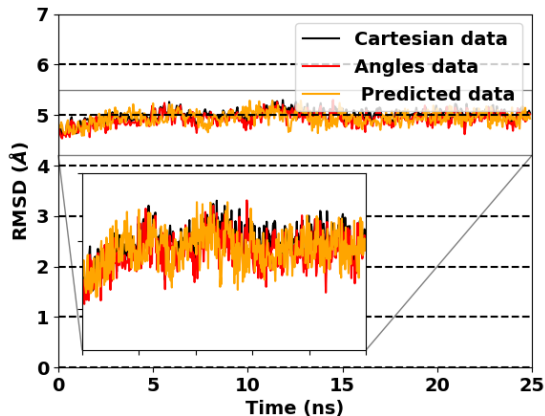
(a) $\tilde{\theta}$ statistics with $n=2$.(b) RMSD with $n=2$.(c) RMSD with $n=5$.

FIG. 4: Statistical performance of angles (upper) and RMSD of CA atoms (lower) in the test datasets. Readers are redirected to CASP14 website for RMSD calculation methods. In the upper figure, the values in the nodes are the mean values and the vertical lines in the node show the standard deviations. In the lower figure, the black line represents rmsds calculated from original trajectories, the red line represents the rmsds obtained from structures re-constructed from CVs and the orange line represents the rmsds from predicted structures.

well with previous structural analysis, where deviations were consistently less than 0.2 angstrom and the average difference using angles ($\Delta\text{RMSD}_{\text{Angle}}(t)$) was 0.0691 angstrom with a standard error of 0.0418 angstrom. Additionally, the predicted trajectories closely resemble the original data, particularly between 15-25 ns and 0-5 ns for $n=2$, as shown by the RMSD profiles. This overall match is also satisfied for $n=5$ with better agreement during 0-5 and around 12 ns, while worse agreement around 10 and 16 ns. A convergence study (Fig. 6, Appendix) explored additional n values (1, 3). As expected, $n = 1$ resulted in significant deviations, indicating insufficient information is learned. Increasing n to 2 eliminated these deviations, suggesting successful information capture. Interestingly, $n = 3$ led to a slight performance decline, while $n = 5$ offered minimal improvement while potentially causing slower training and overfitting. Therefore, $n = 2$ is optimal for convergence. The observed convergence behavior aligns with our prior analysis (Eq. 14), where $n \geq 2$ appears sufficient to capture the essential force field information and generate meaningful data for MD simulations. The close agreement between our predicted and reference RMSD values suggests a more accurate representation of protein dynamics in our coarse-grained method. This is particularly noteworthy because RMSD is highly sensitive to the choice of CVs.

IV. CONCLUSION AND OUTLOOK

This research introduces a novel method using artificial intelligence to perform rapid, coarse-grained simulations of protein molecules. Our approach establishes a two-way link between simplified protein descriptions (CVs) and their detailed 3D structures. This link, built using tree-like coefficients, allows for accurate reconstruction of protein structures. Using a DNN, we successfully generated the MD trajectories of a 168-amino acid target protein (T1027) on a standard computer. This accomplishment is remarkable because it achieves speeds 10,000 times faster than traditional MD simulations, which require powerful supercomputers. Importantly, the generated trajectories closely match the statistical behavior and structural properties observed in real MD simulations. This work paves the way for highly efficient and accurate coarse-grained protein simulations using artificial intelligence.

These future research directions hold significant promise for further refining and expanding the capabilities of the presented framework.

- 1. Enhanced Sampling within the Coarse-Grained Framework.** While our training data incorporates enhanced sampling methods, the network may not fully capture the temperature dependence of the CV space. Future work will explore incorporating temperature and energy information directly into the DNN training process.
- 2. Data Filtering and Separation of Timescales.** Traditional data filtering techniques, such as those implemented in frameworks like PyEMMA³⁴, can potentially

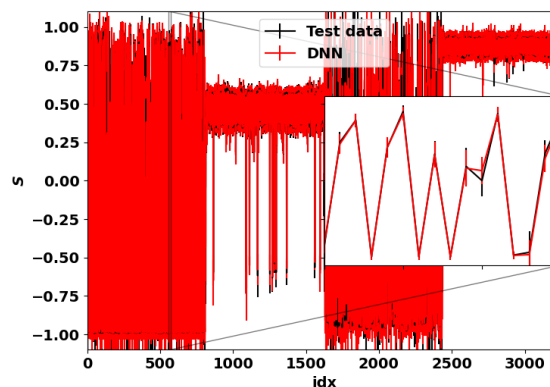


FIG. 5: The error of sine-cosine (S) of angles in MD simulation.

be adapted to separate slow and fast motions within the recorded CV trajectories. The DNN could then be used to predict the slow dynamics, while fast motions could be modeled probabilistically using Gaussian noise, leading to a Monte Carlo-like simulation, as discussed in the beginning of Sec. II B. However, further investigation is needed to determine whether the concept of "slow" and "fast" remains applicable within the CV domain.

- 3. Exploration of Alternative Training Methods.** Graphical Neural Networks (GNNs) offer an intriguing possibility for incorporating the inherent hierarchical structure of proteins into the training process. GNNs may be particularly well-suited for capturing the differential contributions of backbone and side-chain interactions to the overall dynamics.
- 4. Expanding Applicability to Other Systems** The proposed framework has the potential to be extended beyond protein simulations. By utilizing appropriate CV representations, the method could be applied to MD simulations of Deoxyribonucleic acid (DNA), Ribonucleic acid (RNA), and even non-biochemical systems such as polymers and electrolytes in batteries.

Appendix A: Amino hierarchy

Appendix B: DNN errors

- ¹S. A. Hollingsworth and R. O. Dror, "Molecular Dynamics Simulation for All," *Neuron* **99**, 1129–1143 (2018).
- ²M. I. Zimmerman and G. R. Bowman, *Methods in Enzymology*, 1st ed., Vol. 578 (Elsevier Inc., 2016) pp. 213–225.
- ³M. Bergdorf, A. Robinson-Mosher, X. Guo, K.-H. Law, D. E. Shaw, and D. E. Shaw, "Desmond/GPU Performance as of April 2021," **1** (2021).
- ⁴D. E. Shaw, P. J. Adams, A. Azaria, J. A. Bank, B. Batson, A. Bell, M. Bergdorf, J. Bhatt, J. Adam Butts, T. Correi, R. M. Dirks, R. O. Dror, M. P. Eastwo, B. Edwards, A. Even, P. Feldmann, M. Fenn, C. H. Fenton,

TABLE I: Protein Structure Hierarchy (Ignoring Common N Atoms). This figure depicts the hierarchical representation of a protein structure, with each box representing a group of atoms sharing a local coordinate frame. The hierarchy starts with CA atoms in the first column, and progressively incorporates neighboring atoms in subsequent columns (increasing depth, show as 0, 1, 2...6) in the first row.

Amino	0	1	2	3	4	5	6
ALA	CA	CB					
		C	O				
VAL	CA	CB	CG1,CG2				
		C	O				
LEU	CA	CB	CG	CD1,CD2			
		C	O				
GLY	CA	C	O				
ILE	CA	CB	CG1				
		C	O	CG2	CD		
MET	CA	CB	CG	SD	CE		
		C	O				
TRP	CA	CB	CG	CD1,CD2	NE1,CE2		
		C	O	CE3,CZ2	CZ3,CH2		
PHE	CA	CB	CG	CD1,CD2	CE1,CE2		
		C	O	CZ			
PRO	CA	CB	CG,CD				
		C	O				
SER	CA	CB	OG				
		C	O				
CYS	CA	CB	SG				
		C	O				
ASN	CA	CB	CG	OD1,ND2			
		C	O				
GLN	CA	CB	CG	CD	OE1,OE2		
		C	O				
THR	CA	CB	OG1,CG2				
		C	O				
TYR	CA	CB	CG	CD1,CE1	CZ,OH		
		C	O	CE2,CD2			
ASP	CA	CB	CG	OD1			
		C	O	OD2			
GLU	CA	CB	CG	CD	OE1		
		C	O		OE2		
LYS	CA	CB	CG	CD	CE	NZ	
		C	O				
ARG	CA	CB	CG	CD	NE	CZ	NH1,NH2
		C	O				
HIS	CA	CB	CG	ND1,CD2			
		C	O	CE1,NE2			

Appendix C: Convergence study

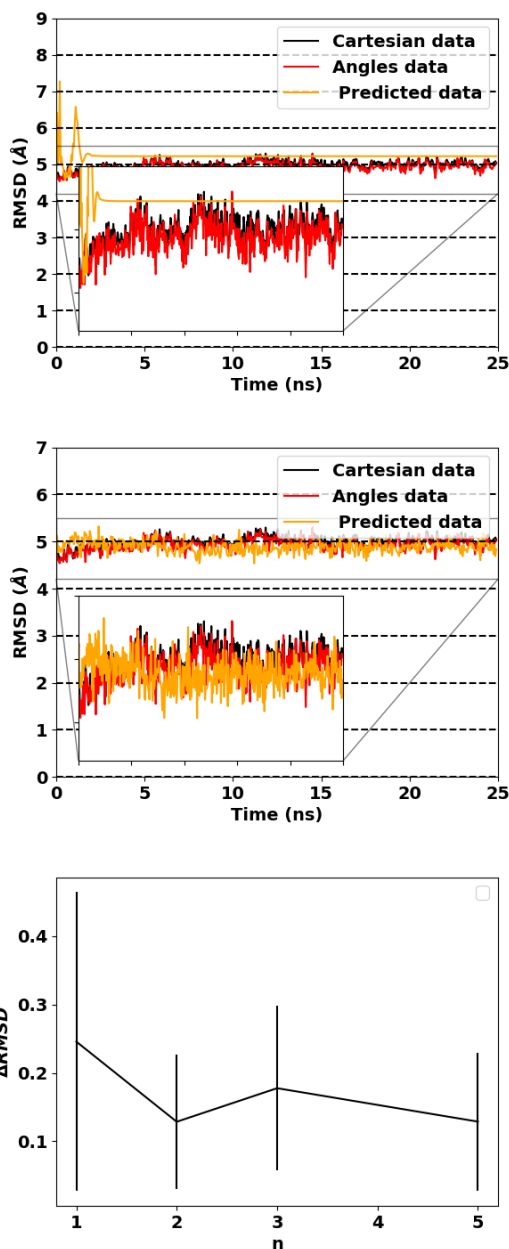


FIG. 6: RMSD profiles from model trained with (first) $n=1$ and (second) 3, respectively, and (third) convergence profile for $n=1-5$.

A. Forte, J. Gagliardo, G. Gill, M. Gorlatova, B. Greskamp, J. P. Grossman, J. Gullingsrud, A. Harper, W. Hasenplaugh, M. Heily, B. C. Heshmat, J. Hunt, D. J. Ierardi, L. Iserovich, B. L. Jackson, N. P. Johnson, M. M. Kirk, J. L. Klepeis, J. S. Kuskin, K. M. Mackenzie, R. J. Mader, R. McGowen, A. McLaughlin, M. A. Moraes, M. H. Nasr, L. J. Nociolo, L. O'Donnell, A. Parker, J. L. Peticolas, G. Pocina, C. Predescu, T. Quan, J. K. Salmon, C. Schwink, K. S. Shim, N. Siddique, J. Spengler, T. Szalay, R. Tabladillo, R. Tartler, A. G. Taube, M. Theobald, B. Towles, W. Vick, S. C. Wang, M. Wazlowski, M. J. Weingarten, J. M. Williams, and K. A. Yuh, "Anton 3: Twenty Microseconds of Molecular Dynamics Simulation before Lunch,"

- International Conference for High Performance Computing, Networking, Storage and Analysis, SC, 1–11 (2021).
- ⁵R. C. Bernardi, M. C. Melo, and K. Schulten, “Enhanced sampling techniques in molecular dynamics simulations of biological systems,” *Biochimica et Biophysica Acta - General Subjects* **1850**, 872–877 (2015).
- ⁶W. G. Noid, “Perspective: Coarse-grained models for biomolecular systems,” *Journal of Chemical Physics* **139** (2013), 10.1063/1.4818908.
- ⁷A. Liwo, C. Czaplewski, J. Pillardy, and H. A. Scheraga, “Cumulant-based expressions for the multibody terms for the correlation between local and electrostatic interactions in the united-residue force field,” *Journal of Chemical Physics* **115**, 2323–2347 (2001).
- ⁸C. Mím, H. Cui, J. A. Gawronski-Salerno, A. Frost, E. Lyman, G. A. Voth, and V. M. Unger, “Structural basis of membrane bending by the N-BAR protein endophilin,” *Cell* **149**, 137–145 (2012).
- ⁹J. W. Chu and G. A. Voth, “Allostery of actin filaments: Molecular dynamics simulations and coarse-grained analysis,” *Proceedings of the National Academy of Sciences of the United States of America* **102**, 13111–13116 (2005).
- ¹⁰A. Yu, A. J. Pak, P. He, V. Monje-Galvan, L. Casalino, Z. Gaieb, A. C. Dommer, R. E. Amaro, and G. A. Voth, “A multiscale coarse-grained model of the SARS-CoV-2 virion,” *Biophysical Journal* **120**, 1097–1104 (2021).
- ¹¹G. Tóth, “Effective potentials from complex simulations: a potential-matching algorithm and remarks on coarse-grained potentials,” *Journal of Physics: Condensed Matter* **19**, 335222 (2007).
- ¹²W. Li and S. Takada, “Characterizing protein energy landscape by self-learning multiscale simulations: Application to a designed β -hairpin,” *Biophysical Journal* **99**, 3029–3037 (2010).
- ¹³J. Wang, S. Olsson, C. Wehmeyer, A. Pérez, N. E. Charron, G. De Fabritiis, F. Noé, and C. Clementi, “Machine Learning of Coarse-Grained Molecular Dynamics Force Fields,” *ACS Central Science* **5**, 755–767 (2019), arXiv:1812.01736.
- ¹⁴B. E. Husic, N. E. Charron, D. Lemm, J. Wang, A. Pérez, M. Majewski, A. Krämer, Y. Chen, S. Olsson, G. De Fabritiis, F. Noé, and C. Clementi, “Coarse graining molecular dynamics with graph neural networks,” *Journal of Chemical Physics* **153**, 1–16 (2020), arXiv:2007.11412.
- ¹⁵L. Zhang, H. Wang, and E. Weinan, “Reinforced dynamics for enhanced sampling in large atomic and molecular systems,” *Journal of Chemical Physics* **148** (2018), 10.1063/1.5019675, arXiv:1712.03461.
- ¹⁶D. Wang, Y. Wang, J. Chang, L. Zhang, H. Wang, and W. E, “Efficient sampling of high-dimensional free energy landscapes using adaptive reinforced dynamics,” *Nature Computational Science* **2**, 20–29 (2022), arXiv:2104.01620.
- ¹⁷G. Xu, Q. Wang, and J. Ma, “OPUS-Rota4: a gradient-based protein side-chain modeling framework assisted by deep learning-based predictors,” *Briefings in Bioinformatics* **23**, 1–10 (2022).
- ¹⁸G. Xu, Z. Luo, R. Zhou, Q. Wang, and J. Ma, “OPUS-Fold3: a gradient-based protein all-atom folding and docking framework on TensorFlow,” *Briefings in Bioinformatics* **24**, 1–8 (2023).
- ¹⁹J. Jumper, R. Evans, A. Pritzel, T. Green, M. Figurnov, O. Ronneberger, K. Tunyasuvunakool, R. Bates, A. Židek, A. Potapenko, A. Bridgland, C. Meyer, S. A. Kohl, A. J. Ballard, A. Cowie, B. Romera-Paredes, S. Nikolov, R. Jain, J. Adler, T. Back, S. Petersen, D. Reiman, E. Clancy, M. Zielinski, M. Steinegger, M. Pacholska, T. Berghammer, S. Bodenstein, D. Silver, O. Vinyals, A. W. Senior, K. Kavukcuoglu, P. Kohli, and D. Hassabis, “Highly accurate protein structure prediction with AlphaFold,” *Nature* **596**, 583–589 (2021).
- ²⁰J. Köhler, Y. Chen, A. Krämer, C. Clementi, and F. Noé, “Flow-Matching: Efficient Coarse-Graining of Molecular Dynamics without Forces,” *Journal of Chemical Theory and Computation* **19**, 942–952 (2023), arXiv:2203.11167.
- ²¹J. Parsons, J. B. Holmes, J. M. Rojas, J. Tsai, and C. E. M. Strauss, “Practical Conversion from Torsion Space to Cartesian Space for In Silico Protein Synthesis,” *Wiley InterScience* **0211458** (2005), 10.1002/jcc.20237.
- ²²J. Zhu, “Theoretical investigation of the Freeman resonance in the dissociative ionization of H₂⁺,” *Physical Review A* **103**, 013113 (2021).
- ²³J. Zhu and A. Scrinzi, “Electron double-emission spectra for helium atoms in intense 400-nm laser pulses,” *Physical Review A* **101**, 063407 (2020).
- ²⁴J. Zhu, “Quantum simulation of dissociative ionization of H₂⁺ in full dimensionality with a time-dependent surface-flux method,” *Physical Review A* **102**, 053109 (2020).
- ²⁵J. Moulton, “A decade of CASP: Progress, bottlenecks and prognosis in protein structure prediction,” *Current Opinion in Structural Biology* **15**, 285–289 (2005).
- ²⁶J. Moulton, J. T. Pedersen, R. Judson, and K. Fidelis, “A large-scale experiment to assess protein structure prediction methods,” *Proteins: Structure, Function, and Bioinformatics* **23**, ii–iv (1995).
- ²⁷D. Van Der Spoel, E. Lindahl, B. Hess, G. Groenhof, A. E. Mark, and H. J. Berendsen, “GROMACS: Fast, flexible, and free,” *Journal of Computational Chemistry* **26**, 1701–1718 (2005).
- ²⁸E. Lindahl, B. Hess, and D. van der Spoel, “GROMACS 3.0: A package for molecular simulation and trajectory analysis,” *Journal of Molecular Modeling* **7**, 306–317 (2001).
- ²⁹H. J. Berendsen, D. van der Spoel, and R. van Drunen, “GROMACS: A message-passing parallel molecular dynamics implementation,” *Computer Physics Communications* **91**, 43–56 (1995).
- ³⁰C. Zhang and J. Ma, “Enhanced sampling and applications in protein folding in explicit solvent,” *The Journal of Chemical Physics* **132**, 244101 (2010), arXiv:1003.0464.
- ³¹T. Zang, L. Yu, C. Zhang, and J. Ma, “Parallel continuous simulated tempering and its applications in large-scale molecular simulations,” *The Journal of Chemical Physics* **141**, 044113 (2014).
- ³²T. Zang, T. Ma, Q. Wang, and J. Ma, “Improving low-accuracy protein structures using enhanced sampling techniques,” *The Journal of chemical physics* **149** (2018), 10.1063/1.5027243.
- ³³T. Ma, T. Zang, Q. Wang, and J. Ma, “Refining protein structures using enhanced sampling techniques with restraints derived from an ensemble-based model,” *Protein science : a publication of the Protein Society* **27**, 1842–1849 (2018).
- ³⁴M. K. Scherer, B. Trendelkamp-Schroer, F. Paul, G. Pérez-Hernández, M. Hoffmann, N. Plattner, C. Wehmeyer, J. H. Prinz, and F. Noé, “PyEMMA 2: A Software Package for Estimation, Validation, and Analysis of Markov Models,” *Journal of Chemical Theory and Computation* **11**, 5525–5542 (2015).